Nanoimprint lithography of high-density cobalt dot patterns for fine tuning of dipole interactions

M. Natali,[a] A. Lebib, E. Cambril, and Y. Chen
LPN, CNRS, 196 Avenue Henri Ravera, 92225 Bagneux, Cedex, France

I. L. Prejbeanu and K. Ounadjela
IPCMS, Groupe d'Etude des Matériaux Métalliques, 23 rue du Loess, 67037 Strasbourg, France

(Received 1 June 2001; accepted 8 October 2001)

A trilayer nanoimprint process was used to fabricate high-density Co dot arrays. It is shown that choosing hybrane as the top layer resist gives better dimensional control of the replicated patterns compared to PMMA. By adjusting the etching time in the transfer process the dot sizes could be tailored in a wide range. The fabricated dot arrays with different sizes and period have then been studied by magneto-optic and magnetic-force microscopy measurements. The magnetization reversal was found to occur through vortex nucleation/annihilation. Dipolar interactions were clearly identified both in arrays with constant dot diameter and variable period and in arrays with fixed period and variable dot diameters. In the case of closely packed dots vortex chain structures along the field direction can be formed as a consequence of a nucleation cascade process. © *2001 American Vacuum Society.* [DOI: 10.1116/1.1421573]

I. INTRODUCTION

Nanoimprint lithography appears as a promising low-cost, high-throughput technique for fabrication of sub-100-nm-scale features and has been successfully applied ''for instance'' to fabricate ring transistors[1] and ultra-high-density magnetic storage media.[2] Basically, nanoimprint lithography involves a physical deformation of a thin layer of polymer deposited on a substrate by using a rigid mold, followed by a pattern transfer involving the complete removal of the residual polymer in the recessed areas of the pattern. While the imprinting process with a single-layer polymer is suitable for many applications, the so-called bilayer and trilayer techniques[3,4] are preferred to obtain resist patterns with higher aspect ratio. This is the case when magnetic dots with relatively large thickness are fabricated by metal deposition and lift-off.

In the present work, we compare the performance of trilayer nanoimprint using as a top layer resist either PMMA or a hyperbranched polymer, named hybrane.[5] Hybrane is found to yield better size control and more uniform imprinting than PMMA. By adjusting the etching time in the transfer process the size of the patterns could be tailored. High-density arrays of Co nanomagnets are fabricated and investigated to evaluate dipolar interactions among the dots. Magnetization reversal was found to take place by nucleation and subsequent annihilation of magnetic vortices. We show that the vortex nucleation and annihilation fields are altered in accordance with a simple dipolar interaction term both for arrays with constant dot diameter and variable period as well as for arrays with fixed period and variable dot diameter. In the case of closely packed dots, chain structures along the field direction can be formed as a consequence of a nucleation cascade process.

[a]Electronic mail: marco.natali@12m.cnrs.fr

II. EXPERIMENT

A mold for imprinting was fabricated by electron-beam lithography and reactive ion etching (RIE) from a thermally oxidized silicon wafer. The patterns on the mold had a height of 155 ± 5 nm as determined from a profilometer scan. The patterns include arrays of circular dots with diameters $D=100$, 200, 500, and 1000 nm. For each dot diameter arrays with different array periods P were present. Period/diameter ratios ranged from $P/D=1.1$ to $P/D=3/1$. Each array had a size of 150×150 μm^2. The mold is spin coated with a thin layer of a release agent.

The trilayer resist system used consisted of a bottom layer of PMGI about 200 nm thick, a 10-nm-thick Ge middle layer and a top layer of either hybrane—a novel hyperbranched polymer with a glass transition temperature $T_g=70\,^{\circ}C$—or PMMA with a molecular weight of 950 kg/mol and $T_g=125\,^{\circ}C$. Imprinting was performed at 140 °C and a pressure of 80 bar for 30 min. At this temperature, the bottom PMGI layer is thermally stable so that deformation takes place only in the top layer. The pattern can then be transferred to the middle and bottom layers with conventional RIE techniques. We used O_2 gas to remove the residue of the top layer imprinted area with a gas flow rate of 10 sccm, a pressure of 5 mTorr, and a power of 10 mW. Afterwards, the patterned top layer is used as mask for a second RIE to etch Ge with SF_6 at a gas flow rate of 10 sccm, a pressure of 30 mTorr, and a power of 60 mW. Finally, Ge is used as a mask for a third RIE to etch the PMGI bottom layer with O_2 of 10 sccm gas flow rate, 5 mTorr pressure, and 10 mW power. The imprinted resist patterns are characterized by Dektak profilometer scans and scanning electron microscopy.

Cobalt dots are fabricated by rf sputter deposition and lift-off. Magnetic characterization was performed by magneto-optical Kerr effect (MOKE) measurements. Hysteresis loops in the longitudinal geometry were recorded at

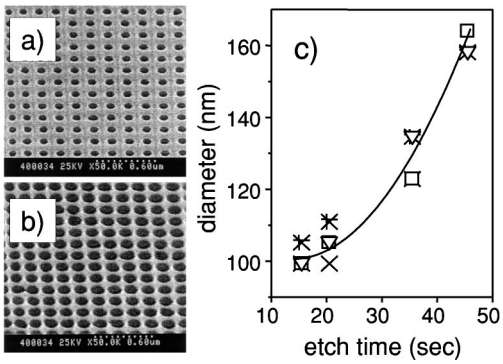

FIG. 1. SEM images of PMGI resist patterns obtained from trilayer nanoimprint: (a) hybrane etching time 15 s, (b) hybrane etching time 45 s, and (c) diameter of PMGI holes as a function of hybrane etching time. Different symbols represent results obtained with the same imprint but different etch times.

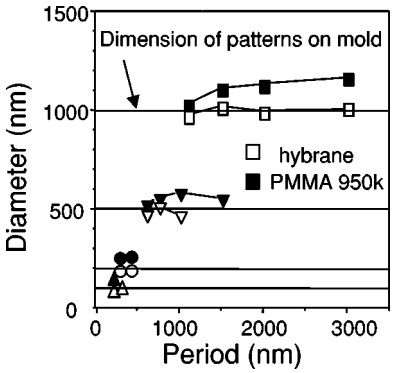

FIG. 2. Diameter of holes in PMGI resist patterns for arrays with different array period and nominal hole diameter (horizontal lines).

room temperature. Magnetic-force microscopy (MFM) was performed in the phase detection mode (Nanoscope Dimension 3100) using CoCr-coated Si cantilever tips. Images were recorded at a lift height of 100 nm. A magnetic field was applied by two small movable permanent magnets mounted on the sample stage.

III. RESULTS AND DISCUSSION

Scanning electron microscopy (SEM) images of PMGI patterns obtained with our process using hybrane as the top layer are shown in Figs. 1(a) and 1(b). The holes with diameters $D=100$ nm (a) and $D=160$ nm (b) were obtained from the same mold pattern by choosing different etching times of the hybrane layer. We remember that the role of the etching is to remove the residual hybrane layer at the bottom of the embossed structures. When the etching time exceeds that required to remove the residual layer, lateral etching becomes important, resulting in an increase in the pattern size, as shown in Fig. 1(c). If the residual layer thickness of hybrane is well controlled, this effect may be used to fine tune the size of the patterns. We found that the whole process can be controlled reproducibly over a wide range of etching times as indicated by the scatter of data points in Fig. 1(c).

An important issue in lithography is the ability to replicate patterns with different dimensions and spacings. In Fig. 2, we show the results obtained by imprinting in a single step arrays with different dot diameters and period. The abscissa gives the measured hole diameter after transfer into the PMGI layer and the ordinate the period of the array of holes. Results obtained with a top layer of hybrane are compared to those obtained using PMMA 950 kg/mol as the top layer. The horizontal lines give the pattern sizes on the mold. Clearly, a deviation of the resist pattern sizes from the mold is observed for PMMA, increasing with period as well as with nominal pattern diameter. On the other hand, for hybrane the resist pattern sizes are almost identical to the mold patterns.

To understand the origin of this difference we measured the residual layer thickness after imprinting. A SEM image of an embossed PMMA layer is shown in Fig. 3(a) and shows a residual layer of about 90 nm at the bottom of the holes. The embossed contrast is 160 nm and closely matches the mold contrast. On the other hand, the total resist thickness from Fig. 3(a) is 260 nm and is larger than the initial thickness, which was 190 nm. The origin of this increase can be understood as follows: as the mold penetrates into the resist the latter is displaced upwards filling up the recessed parts of the mold, therefore, giving an increase in the uppermost resist level. In Fig. 3(b) we show schematically a resist pattern for an imprinted array of finite size. It can be seen that the height enhancement ΔH we mentioned before may be determined by performing a profilometer scan across the array. The residual layer thickness h_r can then be obtained from the relation $h_r=h_i+\Delta H-h_m$. Here, h_i, h_m are the initial thickness and the mold contrast and are defined in Fig. 3(b). We thus determined h_r for different arrays in both cases of PMMA [Fig. 3(c)] and hybrane [Fig. 3(d)]. For PMMA, the residual layer thickness is dependent on the spacing as well as on the nominal size of the patterns. This is in contrast to the case of hybrane where an almost constant residual

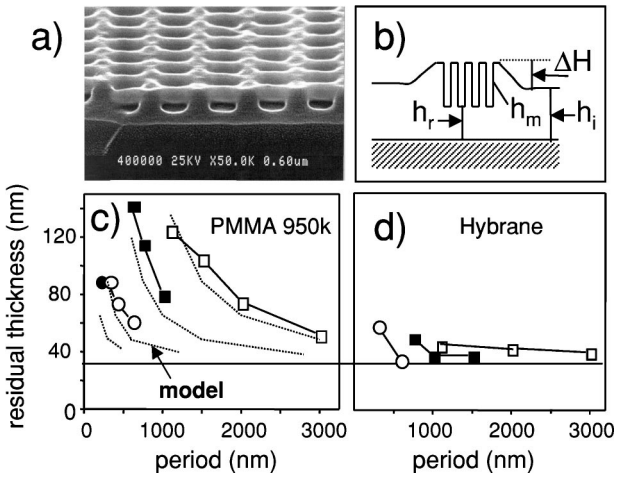

FIG. 3. (a) SEM image of embossed PMMA layer. (b) Schematic illustration of a resist layer after embossing. (c) and (d) Residual resist layer thickness at the bottom of embossed holes as a function of array period for different mold pattern diameters: open squares $D=1$ μm, full squares $D=500$ nm, open circles $D=200$ nm, and full circle $D=100$ nm.

layer thickness is found. The different behavior of h_r can be easily explained by considering the much different glass transition temperature of hybrane and PMMA. The lower viscosity of hybrane at the imprinting temperature allows the polymer to escape from the patterned area into the surrounding unpatterned region. In this case the height enhancement ΔH in Fig. 3(b) tends to zero so that the residual layer thickness tends to $h_r = h_i - h_m = 35$ nm in our case, in good agreement with Fig. 3(d). For PMMA, however, the relatively high viscosity prevents the evacuation of the resist so that h_r is determined by conservation of the resist volume during imprinting. Assuming A_p, A_r as the areas of protruding and recessed parts of the mold inside the patterned region the conservation of resist volume is expressed by

$$h_i(A_p + A_r) = (A_p + A_r)h_r + A_r h_m . \quad (1)$$

For dots with diameter D and array period P: $A_p = \pi D^2/4$ and $A_r = P^2 - A_p$. The residual layer thickness may be determined as a function of P and D. The experimental data points in Fig. 3(c) show a good match with the curves corresponding to Eq. (1), proving the correctness of the above picture.

We then note that in order to transfer all patterns of the PMMA layer into the Ge and PMGI layers the etching time of PMMA must be adjusted to remove the thickest residual layer in Fig. 3(c), i.e., 140 nm. This was achieved by etching for 55 s with O_2 plasma. By extrapolating the curve in Fig. 1(c) to 55 s, this should give an increase of hole diameter of 140 nm, which agrees reasonably with the maximum deviation in Fig. 2. We conclude that hybrane permits a better size control during pattern transfer in our trilayer system.

As an application, we fabricated arrays of cobalt dots by sputtering deposition and lift-off. It is expected that magnetic dipole interactions in arrays of closely spaced dots play an important role in the magnetization reversal process. Previously, dipolar interactions have been studied in square lattices of perpendicularly magnetized dots.[6,7] An antiferromagnetic-type ''checkerboard'' ground state was observed, where neighboring magnets tend to be magnetized in opposite directions. For in-plane magnetized dots a narrowing of the switching field distribution by dipolar interactions was observed as well as a quadratic in-plane anisotropy related to the array symmetry.[8,9] We show here the dependence of dipolar interactions as a function of array period and dot diameter in high-density Co dot arrays.

In Fig. 4 a MOKE hystersis loop is shown for dots with $D = 500$ nm and $P = 1500$ nm. The dots are in-plane magnetized and the loop shape suggests a magnetization reversal via a flux-closure configuration: as the field is decreased starting from negative saturation net magnetization is lost at a critical field H_n and is almost zero at remanence. This is typical of flux-closure configurations where the magnetization turns circularly inside the dot. Indeed, MFM images performed for a field at point II of the loop revealed the typical contrast of magnetic vortices,[10] as shown in Fig. 4(b) II. On the other hand, at saturation the dots are found in a uniformly magnetized single-domain (SD) state having a dipole like contrast, as shown in Fig. 4(b) I. As the field

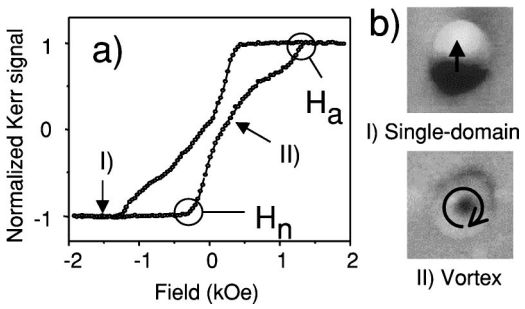

FIG. 4. (a) MOKE hysteresis loop of an array of Co dots with $D = 500$ nm, $P = 1500$ nm, and thickness 30 nm. (b) MFM images of single-domain state (I) and vortex state (II).

increases towards positive values starting from point II of the loop, magnetization reappears, and finally, the vortex is annihilated at the field H_a. In Fig. 5 we plot H_n and H_a versus the array period for dots with $D = 500$ nm. Both H_a and H_n decrease in absolute value as the distance between the dots decreases. This can be understood in terms of dipolar interactions among the dots as follows: the aligned dipole moments of SD states in the saturated state stabilize each other and thus retard vortex nucleation. For the same reason the coupling between the dots induces anticipation of vortex annihilation. To quantitatively verify this interpretation we consider the dipole interaction field in a square array of uniformly magnetized SD dots which is given by[11]

$$H_{\mathrm{dip}} = 4.2 M_s V / P^{-3}, \quad (2)$$

where $M_s = 1420\ \mathrm{emu\ cm^{-3}}$ is the saturation magnetization density of cobalt and V the dot volume. This field adds to the external field, and hence, determines the observed shift of H_n and H_a. By fitting the experimental data points in Fig. 5 with an expression of type $A + 4.2\mu P^{-3}$, with A and μ as fitting parameters, we obtain $\mu = 13 \pm 3 \times 10^{-12}$ emu, which agrees reasonably well with the expected value $\mu = M_s V = 8.4 \times 10^{-12}$ emu. In Fig. 6 we analyze the dependence of H_n on dot diameter. Open circles represent samples of widely spaced dots with $P = 3D$ and full circles samples with constant $P = 200$ nm. The latter samples were obtained by exploiting the overetching effect described in Fig. 1. In both cases, the vortex nucleation field increases with increasing

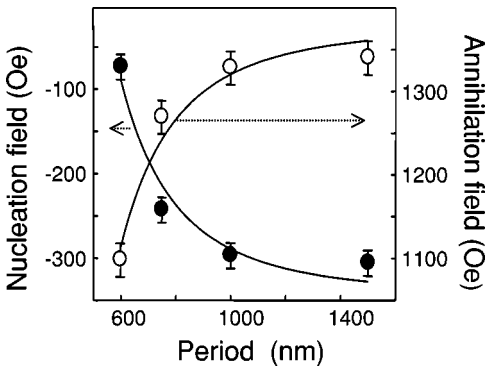

FIG. 5. Variation of the vortex nucleation and annihilation fields with array period for arrays with $D = 500$ nm, and thickness 30 nm.

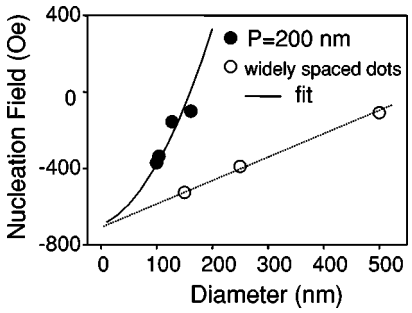

FIG. 6. Variation of the vortex nucleation field with dot diameter for widely spaced dots ($P=3D$) and for dots with $P=200$ nm. The continuous lines give fits to the data points and are described in the text.

dot diameter. The origin of this trend can be understood qualitatively as follows: the driving force for vortex nucleation is the demagnetization field, which is formed by the magnetic surface charge density $\rho=\mathbf{M}_s\circ\mathbf{n}$, where $\mathbf{n}$ is the surface normal to the dot border. Since the magnetic field due to these charges decays towards the dot center, larger dots have a smaller demagnetization field than smaller dots and, therefore, nucleate vortices ''later.'' For dots with constant P, however, the increase of H_n with D is more pronounced than for widely spaced dots with $P=3D$. This, of course, is again related to dipolar coupling between the dots. The quantitative analysis in this case must take into account the superposition of an intrinsic ''demagnetization'' induced shift and a dipolar shift. We, therefore, fit the data points with an expression of the type $AD+4.2M(\pi D^2t/4)P^{-3}$, where A is obtained from a linear fit to the data points of widely spaced dots. The dot thickness is t and M is the effective magnetization density of the dots. From the fit we find $M=1600\pm100\,\mathrm{emu\,cm^{-3}}$, in reasonable agreement with the expected value for Co.

We, moreover, investigated the spatial distribution of vortex and SD states during vortex nucleation by recording MFM images as a function of applied field. A sample with $D=500$ nm, $P=600$ nm, and $t=50$ nm was first saturated and then MFM images recorded after decreasing the field. A MFM image recorded at 100 Oe is shown in Fig. 7. The field is applied along an array axis. SD dots are recognized by the characteristic dipole contrast with black and white ends aligned along the field direction in Fig. 7, whereas vortex dots in this low-resolution image appear without magnetic contrast. It can be noted that the SD dots are aggregated in the form of chains along the field direction. Since in the initial state all dots were in a SD state this indicates that vortices have nucleated in the form of chains aligned with the applied field. Such vortex chain structures were not observed for widely spaced dots, where the distribution of SD and vortex states was random. The physical mechanism leading to such a correlation can be understood in terms of dipolar interaction as follows: starting from saturation when a dot switches to the vortex state the neighboring dots, which lie in the direction of the applied field, begin to ''feel'' a lower interaction field than average, due to the loss of the dipole moment of the vortex dot. Therefore, they are favored to switch to the vortex state. The process then repeats in a cascade-like fashion determining chains of vortices aligned along the field direction.

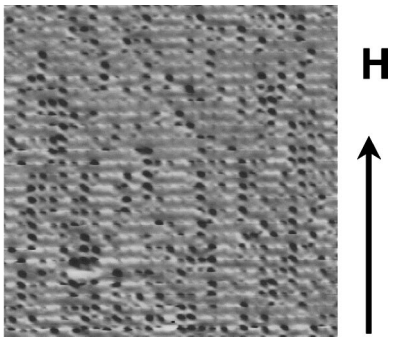

FIG. 7. MFM image showing the distribution of vortex and single-domain states in an array of Co dots with $D=500$ nm, $P=600$ nm, and thickness 50 nm. A field of 100 Oe is applied along an array axis in the plane of the sample (arrow). The scan size is 20×20 μm.

IV. CONCLUSION

We have shown that high-density Co dot arrays with a very high filling factor can be fabricated by using a trilayer nanoimprint technique. Using hybrane as the top layer resist gives better dimensional control of the replicated patterns compared to PMMA and permits fine tuning of the size of the patterns by adjusting the etching time in the transfer process. Cobalt dot arrays with different diameters and periods were characterized magnetically and dipolar interactions among the dots were demonstrated as a function of both array period and dot diameter. The magnetization reversal process was observed to occur by nucleation/annihilation of magnetic vortices. In the case of closely packed dots vortex chain structures along the field direction can be formed as a consequence of a nucleation cascade process.

[1]S. Y. Chou, P. R. Krauss, and P. J. Renstrom, J. Vac. Sci. Technol. B **14**, 4129 (1996).
[2]P. R. Krauss and S. Y. Chou, J. Vac. Sci. Technol. B **13**, 2850 (1995).
[3]B. Faircloth, H. Rohrs, R. Tiberio, R. Ruoff, and R. R. Krchnavek, J. Vac. Sci. Technol. B **18**, 1866 (2000).
[4]Y. Chen, A. Lebib, S. Li, A. Pépin, D. Peyrade, M. Natali, and E. Cambril, Eur. Phys. J.: Appl. Phys. **12**, 223 (2000).
[5]Hybrane is a collective name for a set of hyperbranched polymers that are prepared by polycondensating cyclic anhydrides with diisopropanolamine. The product is a poly-amide-ester with multiple alcohol endgroups that can be functionalized with carboxylic acids. The particular Hybrane material we used was selected because of its glass transition temperature of ~70 °C. For further information, see R. A. T. M. van Benthem, D. Muscat, and D. A. W. Stanssens, in PMSE (Polymeric Materials Science and Engineering), Proceedings of the American Chemical Society Division of Polymeric Materials: Science and Engineering (1999), Vol. 80, pp. 72–73, and the internet site www.dsm.nl/hybrane (unpublished).
[6]T. Aign, P. Meyer, S. Lemerle, J. P. Jamet, J. Ferré, V. Mathet, C. Chappert, J. Gierak, C. Vieux, F. Rousseaux, H. Launois, and H. Bernas, Phys. Rev. Lett. **81**, 5656 (1998).
[7]M. Hwang, M. C. Abraham, A. Savas, H. I. Smith, R. J. Ram, and C. A. Ross, J. Appl. Phys. **87**, 5108 (2000).
[8]G. A. Gibson and S. Schultz, J. Appl. Phys. **73**, 4516 (1993).

[9]C. Mathieu, C. Hartman, M. Bauer, O. Buettner, S. Riedling, B. Roos, S. O. Demokritov, B. Hillebrands, B. Bartelian, C. Chappert, D. Decanini, F. Rousseaux, E. Cambril, A. Mueller, B. Hoffman, and U. Hartmann, Appl. Phys. Lett. **70**, 2912 (1993).

[10]T. Shinjo, T. Okuno, R. Hassdorf, K. Shigeto, and T. Ono, Science **289**, 930 (2000).

[11]M. Grimdisch, Y. Jaccard, and I. K. Schuller, Phys. Rev. B **58**, 11539 (1998).